Towards *Mycobacterium tuberculosis* detection at the point-of-care: a brighter solvatochromic probe permits the detection of mycobacteria within minutes

Mireille Kamariza[1,], Samantha G. L. Keyser[2,*], Ashley Utz[1], Benjamin D. Knapp[3], Green Ahn[4], Christopher J. Cambier[4], Teresia Chen[2], Kerwyn Casey Huang[3,5,6,7], Carolyn R. Bertozzi[2,4,8,†]*

Author Affiliations

[1]Department of Biology, Stanford University, Stanford, CA 94305, USA

[2]Department of Chemistry, University of California, Berkeley, Berkeley, CA 94720, USA

[3]Biophysics Program, Stanford University, Stanford, CA 94305, USA

[4]Department of Chemistry, Stanford University, Stanford, CA 94305, USA

[5]Department of Bioengineering, Stanford University, Stanford, CA 94305, USA

[6]Department of Microbiology and Immunology, Stanford University School of Medicine, Stanford, CA 94305, USA

[7]Chan Zuckerberg Biohub, San Francisco, CA 94158, USA

[8]Howard Hughes Medical Institute, Stanford University, Stanford, CA 94305, USA

*These authors contributed equally.

[†]All correspondence should be addressed to bertozzi@stanford.edu

ABSTRACT

There is an urgent need for point-of-care tuberculosis (TB) diagnostic methods that are fast, inexpensive, and operationally simple. Here, we report on a bright solvatochromic dye trehalose conjugate that specifically detects *Mycobacterium tuberculosis* (Mtb) in minutes. 3-hydroxychromone (3HC) dyes, known to yield high fluorescence quantum yields, exhibit shifts in fluorescence intensity in response to changes in environmental polarity. We synthesized two analogs of 3HC-trehalose conjugates (3HC-2-Tre and 3HC-3-Tre) and determined that 3HC-3-Tre has exceptionally favorable properties for Mtb detection. 3HC-3-Tre-labeled mycobacterial cells displayed a 10-fold increase in fluorescence intensity compared to our previously reports on the dye 4,4-*N,N*-dimethylaminonapthalimide (DMN-Tre). Excitingly, we detected fluorescent Mtb cells within 10 minutes of probe treatment. Thus, 3HC-3-Tre permits rapid visualization of mycobacteria that ultimately could empower improved Mtb detection at the point-of-care in low-resource settings.

INTRODUCTION

With 1.2 million deaths and 10 million new cases in 2018, tuberculosis (TB) is the most lethal infectious disease in the world (1). Early detection of the bacterium *Mycobacterium tuberculosis* (Mtb), the causative agent of TB, followed by appropriate treatment could prevent most deaths (2). The gold standard for TB diagnosis remains a labor-intensive culture test that requires weeks of incubation time in specialized facilities. Although more rapid tests are available, they present several important limitations. PCR-based tests are expensive and require skilled technicians. Microscopy-based methods are attractive in low-resource settings as they are low-cost, have fast turnaround times, and report on people at greatest risk of transmission and death (3). As a result, the sputum smear microscopy test is the most widely used technique for TB diagnosis. The century-old smear test is based on the susceptibility of fluorescent auramine dye or colored Ziehl-Neelson (ZN) stain to accumulate within the highly hydrophobic mycobacterial cell wall (4–7). While effective for identification of Mtb cells, this process requires multiple wash steps to reduce non-specific background fluorescence, or in the case of the ZN test, a rigorous counterstaining procedure so that stained Mtb cells can be visualized (8,9). Moreover, the smear test does not distinguish live from dead cells, and this capability is vital in order to assess treatment efficacy early and accurately (2).

In the last decade, we and others have leveraged the trehalose metabolism of mycobacteria to mark them for detection by various imaging methods (10–20). Exogenous trehalose molecules can be directly mycolylated at the 6 position by antigen 85 (Ag85) enzymes to form trehalose monomycolates (TMM) that are inserted into the mycobacterial cell wall, termed the mycomembrane (10). Researchers have shown that Ag85 enzymes are promiscuous enough to tolerate perturbations of varying sizes such as azide (11), alkyne (12), fluorine (13–15), and fluorophore (13,16) groups that permit visualization of the mycomembrane as long as the cell is metabolically active. However, these fluorescent probes require extensive washing before imaging in order to reduce background signal.

Fluorogenic probes, i.e. probes that turn on when metabolized in cells, have proven better suited for TB detection as they require minimal processing. Previous studies have used quenched trehalose fluorophores that become unquenched by Ag85 activity, allowing visualization of growing mycobacterial cells in real-time (17). A dual enzyme-targeting fluorogenic probe allowed the detection of Mtb cells within an hour using a microfluidic system (18). In addition, we reported on a solvatochromic trehalose probe (DMN-Tre) that can detect live Mtb cells in TB patient sputum samples (19). Solvatochromic dyes change their color or fluorescence intensity based on the polarity of the solvent. As a result, these compounds are advantageous for monitoring changes

in hydrophobicity of a molecule of interest (20). Upon acylation of DMN-Tre by Ag85 and insertion of the corresponding trehalose monomycolate (TMM) analog into the mycomembrane, dye fluorescence is turned on, which allows the detection of live mycobacteria with a fluorescence microscope (**Figure 1A**) (19,21). In this context, DMN-Tre has many favorable properties for point-of-care deployment: its operationally simple procedure does not require any wash steps, and it is synthetically convenient and chemically stable. However, the DMN dye is a fluorophore of relatively low brightness, with a molar extinction coefficient of 8800 M^{-1} cm^{-1} in TBS buffer (20) and a low quantum yield of fluorescence in low-dielectric solvents (0.288 in DMF) (22). Consequently, in practice we found that: 1) low-powered fluorescence microscopes currently available in TB health centers may miss labeled cells, and 2) Mtb cells must be labeled with DMN-Tre for at least one hour to achieve detectable levels of fluorescence using standard clinical fluorescence microscopes.

To address these obstacles for point-of-care TB detection, we aimed to develop probes that are brighter and enable faster detection of live Mtb cells. Here, we report the development of a brighter solvatochromic trehalose probe, based on the 3-hydroxychromone (3HC) dye (**Figure 1B**). The 3HC trehalose conjugate (termed 3HC-3-Tre) demonstrated high fluorescence turn-on in hydrophobic solvents as well as when incorporated in the mycobacterial cell surface. This labeling was specific to the trehalose moiety and was detectable without any wash steps. Additionally, the fluorescence intensity of 3HC-3-Tre was 10-fold brighter than DMN-Tre. Finally, the high signal-to-noise ratio of 3HC-3-Tre permitted simple detection of labeled Mtb cells within 10 minutes. Thus, 3HC-3-Tre reagent permits the rapid visualization of mycobacteria and ultimately, could be used to improve Mtb detection at the point-of-care in low-resources settings.

RESULTS

Synthesis of 3HC solvatochromic dyes bound to trehalose

To design a probe with stronger turn-on fluorescence than DMN, we relied on previously reported solvatochromic dyes that fit our target profile. We identified a highly promising class of solvatochromic dyes that are well characterized, synthetically tractable, and have been used in living systems with minimal perturbations (**Figure 1B**) (20). These dyes are based on a 3-hydroxychromone (3HC) scaffold with the advantage of greater tunability due to their synthetic modularity and high quantum fluorescence yield. Moreover, they are further red-shifted, which may minimize background fluorescence.

We began by synthesizing 6-Br-Ac_7-Tre (**Figure 2**). An Appel reaction using N-bromosuccinimide and triphenylphosphine resulted in a mixture of mono-brominated target

compound (6-Br-Tre), a dibrominated side product (6,6'-dibromo-6,6'-dideoxy-α,α'-trehalose), and unreacted starting material. The crude material was then acetylated and purified to give 6-Br-Ac_7-Tre (**Compound 2**). Next, we considered the synthesis of 3HC dyes, here referred to as 3HC-3 (**Compound 3**) and 3HC-2 (**Compound 4**) (23–26). We followed a previous study (23) to achieve synthesis of the aldehyde precursor to 3HC-2 by reacting 3-diethylaminophenol with bromoacetaldehyde diethyl acetal (**Scheme S1**). The intermediate was purified, then subsequently treated with phosphorus(V) oxychloride and *N,N*-dimethylformamide (DMF) to form the benzofuran and to install an aldehyde at the 2-position via a Vilsmeier-Haack reaction. To synthesize the aldehyde precursor to 3HC-3 (**Compound 3**), we nitrated 2-bromo-9,9-dimethylfluorene at the 7-position, reduced the nitrate to an amine, alkylated the amine using ethyl iodide, and converted the bromine to an aldehyde through a Bouveault reaction. To form 3HC-2 and 3HC-3, each aldehyde was reacted with 2'-hydroxyacetophenone, then treated with hydrogen peroxide to obtain the desired products (**Figure 2B**) (27). Finally, to create the dye-Tre probes, the aromatic hydroxyl group on the dye was deprotonated with potassium carbonate and used to displace the bromine atom on 6-Br-Ac_7-Tre (**Figure 2C**) (28). The crude dye-Ac_7-Tre was then deacetylated with catalytic sodium methoxide and purified to produce the final dye-Tre products in yields ranging from 9-63% over three steps. We also synthesized glucose control compounds in a similar fashion (**Scheme S2**).

3HC-trehalose probes label* Mycobacterium smegmatis *(Msmeg) cells more effectively than DMN-Tre

With these probes in hand, we proceeded to characterize their fluorescence intensities and emission spectra in mixtures with various ratios of dioxane and water. The dyes were excited at the optimal excitation wavelengths (405 nm for DMN-Tre and 3HC-3-Tre, 488 nm for 3HC-2-Tre) and fluorescence intensities were measured over a range of emission wavelengths (**Figure 3**). As expected, all probes displayed increased fluorescence as the amount of dioxane increased. DMN-Tre and 3HC-3-Tre both absorbed most strongly at 405 nm and had comparable fluorescence intensities in each solvent mixture tested, although the spectra for 3HC-3-Tre were slightly red-shifted (**Figure 3A**,**B**). 3HC-2-Tre responded well to excitation at 405 nm and 488 nm, although its fluorescence intensity was less sensitive to changes in hydrophobicity overall (**Figure 3C**). However, because the emission spectra underwent a bathochromic shift as solvent polarity increased, significant differences in intensity still occurred between 500 and 550 nm, the approximate range of wavelengths allowed through the GFP emission filter.

139 We also assessed labeling conditions for *Mycobacterium smegmatis* (Msmeg), a
140 nonpathogenic and fast-growing member of the *Mycobacterium* genus commonly used as a
141 model organism for Mtb. Msmeg cells were grown to an optical density at wavelength 600 nm
142 (OD_{600}) of 0.5, then incubated with 1, 10, or 100 μM of each probe for 1 hour at 37 °C, washed
143 three times, and analyzed by flow cytometry using a variety of excitation and emission filter sets
144 (**Figure 4**). As expected, we observed that all trehalose probes labeled Msmeg in a concentration-
145 dependent manner. As well, 3HC-3-Tre and 3HC-2-Tre-labeled cells reached much higher levels
146 of fluorescence intensity compared to DMN-Tre-labeled bacteria (approximately 10-fold and 100-
147 fold higher for 3HC-3-Tre and 3HC-2-Tre, respectively). While DMN-Tre's fluorescence was
148 optimally detected with 405/525 (ex/em) nm filter sets (**Figure 4A**), we determined that the optimal
149 fluorescence detection filter sets for 3HC-3-Tre and 3HC-2-Tre probes were 405/525 and 488/525
150 nm, respectively (**Figure 4B,C**). Excitingly, even with 10-fold lower concentrations, 3HC-3-Tre-
151 labeled Msmeg cells demonstrated nearly 5-fold greater fluorescence intensity compared to DMN-
152 Tre.
153
154 ***3HC-3-Tre rapidly and stably labels mycobacteria in a trehalose-dependent manner***
155 For the dyes to be useful in the field, the labeling procedure must follow a simple protocol.
156 Thus, we sought to determine whether a wash step is necessary based on the degree of
157 background signal when Msmeg cells are labeled with each trehalose probe, glucose-dye control,
158 or free dye. We incubated Msmeg cells with DMN-Tre, 3HC-3-Tre, or 3HC-2-Tre (along with their
159 respective glucose and sugar-free analogs) for 1 hour at 37 °C and performed fluorescence
160 microscopy either immediately or after a wash step with PBS (**Figure 5**). As anticipated, we
161 observed fluorescent Msmeg cells labeled with DMN-Tre, while the fluorescence of DMN-Glc-
162 labeled Msmeg was washed off with PBS (**Figure 5A**), suggesting that the non-specific turn-on
163 of DMN-Glc molecules is likely due to proximity to Msmeg cells. Surprisingly, we observed no
164 fluorescence with 3HC-3-Glc-labeled Msmeg cells, even in unwashed samples (**Figure 5B,**
165 **Figure S1A**), suggesting that internalization of the probe is required for fluorescence turn-on of
166 3HC-3. Interestingly, we observed labeling of Msmeg cells with 3HC-2 and 3HC-2-Glc, even after
167 washing (**Figure 5C, Figure S1B**), suggesting that 3HC-2 labeling is not specific to the trehalose
168 pathway. Intrigued by this result, we wondered whether the fluorescence labeling of Msmeg from
169 3HC-2 dye conjugates would reflect the known trehalose insertion patterning.
170 Previous studies demonstrated that exogenous trehalose molecules are mycolylated at
171 the 6 position via action of Ag85 enzymes, which are localized at the septa and poles of the cell
172 envelope (10,19). We hypothesized that 3HC-2 labeling occurs in an Ag85-independent manner

173 and therefore would not exhibit polar and septal fluorescence. Using total internal reflection
174 fluorescence (TIRF) microscopy, we placed Msmeg cells into a microfluidic flow cell (Methods),
175 introduced liquid growth medium containing DMN-Tre, 3HC-3-Tre, 3HC-2-Tre, or 3HC-2-Glc, and
176 performed time-lapse microscopy (**Figure 6, Figure S2**). Similar to DMN-Tre, 3HC-3-Tre labeling
177 of Msmeg cells showed septal and polar labeling (**Figure 6A**, top two panels). We observed no
178 enhancement in polar or septal fluorescence localization for Msmeg cells labeled with 3HC-2-Tre
179 or 3HC-2-Glc (**Figure 6A**, bottom two panels), further suggesting that this labeling likely does not
180 depend on the trehalose metabolic pathway.

181 After 30 minutes of labeling, we washed out the exogenous dye and continued to acquire
182 fluorescence images. To address the rate of fluorescence change during labeling and washout,
183 we pooled the total cell fluorescence at each timepoint and quantified the mean total and volume-
184 normalized fluorescence across cells (**Figure 6B**). During labeling, the volume-normalized
185 fluorescence initially increased rapidly and then started to plateau; by 10 min, cells reached ~50%
186 of the labeling at 30 min, confirming rapid labeling of all three probes. During washout, total
187 fluorescence was gradually lost (**Figure 6B**). We fit the washout dynamics to an exponential
188 $I(t) = I_0 + I_1 e^{-\gamma t}$. Washout of DMN-Tre labeling was slow, likely because it depends on
189 mycomembrane turnover (**Figure 6Bi, Figure S2A**). Compared to DMN-Tre, cells labeld with
190 3HC-3-Tre or 3HC-2-Tre exhibited a rate of fluorescence loss γ that was 2.3- and 5.9-fold higher
191 than DMN-Tre, respectively (**Figure 6Bii**,**iii, Figure S2B,C**), suggesting additional labeling
192 mechanisms beyond trehalose synthesis. In particular, the washout time scale for 3HC-2-Tre was
193 $\ln 2/\gamma = 7.4$ min, reflecting trehalose-independent transient binding and/or turn-on. Nonetheless,
194 we confirmed that 3HC-3 and 3HC-3-Glc do not label Msmeg cells (**Figure S2E,F**), indicating the
195 specificity of 3HC-3-Tre for trehalose. Taken together, these data demonstrate 3HC-3-Tre, but
196 not 3HC-2-Tre, is an excellent candidate for the rapid detection of mycobacteria. Moving forward,
197 we focused our efforts on the 3HC-3-Tre probe.
198

199 ***3HC-3-Tre labeling of Msmeg cells is much brighter than DMN-Tre and selective for***
200 ***Actinobacteria***

201 Our next goal was to assess the specificity of 3HC-3-Tre labeling of mycobacteria
202 compared with bacterial species that do not incorporate trehalose into their cell envelopes (**Figure**
203 **7**). We analyzed Msmeg cells incubated with 1, 10, or 100 μM of 3HC-3-Tre or 3HC-3-Glc (as a
204 negative control) for 1 hour at 37 ºC. We found that 100 μM 3HC-3-Tre-labeled cells were 100-
205 fold brighter compared to background (**Figure 7A**). Importantly, in the same conditions, the
206 fluorescence intensity of 3HC-3-Tre-labeled cells was 10-fold greater than that of DMN-Tre-

207 labeled cells (**Figure 7B**), confirming that 3HC-3-Tre is a much brighter option than DMN-Tre. We
208 previously reported that DMN-Tre selectively labeled organisms within the Actinobacteria
209 suborder (16,19). To test whether a similar labeling pattern persisted for 3HC-3-Tre, we labeled
210 Msmeg, *Corynebacterium glutamicum* (Cg), *Bacillus subtilis* (Bs), *Escherichia coli* (Ec) and
211 *Staphylococcus aureus* (Sa) with 100 μM 3HC-3-Tre for 1 hour and analyzed the samples by
212 microscopy and flow cytometry (**Figure 7C,D**). Similar to DMN-Tre, we observed bright labeling
213 of Msmeg and Cg cells, consistent with both of these organisms utilizing trehalose in their cell
214 envelopes. Although not detected by microscopy, there was minimal but significant fluorescence
215 from labeled Bs, Ec, and Sa cells compared to the no-dye control using flow cytometry (**Figure**
216 **7C**), perhaps reflecting a trehalose-independent pathway that led to faster washout of 3HC-3-Tre
217 than DMN-Tre (**Figure 6B**).

218 Finally, we assessed labeling of Mtb with 3HC-3-Tre (**Figure 8**). We labeled Mtb strain
219 H37Ra cells with 100 μM 3HC-3-Tre for 1, 2, or 24 hours and then performed microscopy (**Figure**
220 **8A**). Similar to DMN-Tre, we observed labeling within 1 hour, with little discernible increase in
221 fluorescence intensity over additional time (**Figure 8A**). By flow cytometry, we were able to detect
222 significant fluorescence over background within 10 minutes of Mtb H37Ra labeling with 3HC-3-
223 Tre (**Figure 8B**). In the same conditions, with DMN-Tre we required a minimum of 60 minutes to
224 accurately detect significant fluorescence over background (19), likely due to the weak brightness
225 of the fluorophore.

226

227 **DISCUSSION**

228 Tuberculosis (TB) remains a major global health threat (1). As it stands, poor detection
229 methods have contributed to millions of missed TB diagnoses in high-burden, endemic countries
230 (1,2). Due to the lack of accurate detection tests at the point-of-care, TB transmission rates have
231 been sustained in low-income countries. In this study, we report on a solvatochromic dye
232 trehalose conjugate that can swiftly detect mycobacteria. 3HC-3-Tre is a robust fluorogenic probe
233 that specifically labels Actinobacteria such as Mtb within 10 minutes and can be imaged without
234 any wash steps. In addition to its utility for research, this set of attributes may enable the rapid
235 detection of Mtb in sputum samples in low-resource settings.

236 In future work, it may be possible to develop further red-shifted probes such as Nile-red
237 dyes to minimize background fluorescence and maximize signal-to-background ratio, while
238 maintaining minimal perturbations to mycobacteria. Furthermore, it is easily conceivable to
239 synthesize trehalose moieties conjugated to an assortment of colors that span the fluorescence
240 wavelength range to achieve multimodal labeling of mycobacteria. In addition to trehalose, the

241 dyes could be coupled with other types of bacteria-specific molecules (sugars or amino acids)
242 that would permit visualization of a subject of interest in various biological systems.
243 Beyond the performance of the detection methods, TB diagnoses in low-income
244 environments depend on many factors, such as stability, accessibility, and affordability (2). The
245 solvatochromic dyes are highly stable at room temperature even in temperate environments, can
246 potentially be coupled with a portable florescence detection device, and a reasonable estimate of
247 cost would be less than 40 cents per test. Because of these unique attributes, it is conceivable to
248 use these reagents as mobile biomarkers for TB screening in resource-poor, remote
249 environments. Thus, these novel probes can be used in service of both the scientific community
250 to uncover mycobacterial metabolism, and also the clinical community at large for TB detection in
251 high-burden environments.
252

253 **METHODS**

254 **Fluorescence spectra procedures.** One microliter (μL) of each dye-Tre conjugate (10 mM in
255 water) was added to 1 mL of water or 99.9%, 99%, 95%, 90%, 75%, or 50% 1,4-dioxane in 1 cm
256 x 0.4 cm quartz cuvettes (Starna Cells, Inc. 9F-G-10). Fluorescence data were acquired on a
257 Photon Technology International Quanta Master 4 L-format scanning spectrofluorometer
258 equipped with an LPS-220B 75-W xenon lamp and power supply, an A-1010B lamp housing with
259 an integrated igniter, a switchable 814 photon-counting/analog photomultiplier detection unit, and
260 an MD5020 motor driver. In the associated FelixGX software (v. 4.3.4.2010.6904), spectra were
261 acquired using standard emission scan settings with the exception of the lamp slit widths, which
262 were all set to 1 nm. Compounds were excited at 405, 488, 532, or 561 nm and emission intensity
263 was monitored over 415-600 nm, 500-700 nm, 545-700 nm, or 575-750 nm, respectively. Data
264 were exported as a text file and processed in Excel. Prism 7 (GraphPad) was used to create the
265 figures from the final data.
266

267 **General procedures for bacterial culture inoculation.** Cultures of *Mycobacterium smegmatis*
268 (Msmeg), *Mycobacterium marinum* (Mmar), *Corynebacterium glutamicum* (Cg), *Bacillus subtilis*
269 (Bs), *Escherichia coli* (Ec), and *Staphylococcus aureus* (Sa) were grown as described previously
270 (6). Briefly, Msmeg single colonies were inoculated in BD Difco Middlebrook 7H9 media
271 (supplemented with 10% (v/v) oleate-albumin-dextrose-catalase (OADC) enrichment, 0.5% (v/v)
272 glycerol, and 0.5% (w/v) Tween 80) and incubated at 37 °C overnight. For Cg, Bs, Ec, and Sa,
273 single colonies were inoculated in LB medium. Cg cultures were incubated at 30 °C, and Bs, Ec,
274 and Sa cultures were incubated at 37 °C, all overnight. A 1-mL aliquot of Mmar (stored as a frozen

275 stock in 50% glycerol/50% 7H9 medium) was thawed, then pelleted at 3,300*g* for 3 min. Cells
276 were resuspended in 7H9 media supplemented with 10% (v/v) OADC enrichment, 0.5% (v/v)
277 glycerol, and 0.5% (w/v) Tween 80, and incubated at 33 °C overnight.
278
279 **Metabolic labeling experiments**. Experiments were performed as described previously (6).
280 Briefly, overnight bacterial cultures were grown or diluted to an OD_{600} of 0.5 and aliquoted into
281 Eppendorf tubes. The appropriate amount of stock dye (1 or 10 mM) was added to the aliquots to
282 reach the indicated final concentration. Control samples were treated identically, without the
283 addition of any probes. The bacteria were incubated for 1 h at 37 °C (Msmeg, Bs, Ec, Sa) or 30
284 °C (Cg). At the end of the experiment, samples were analyzed by microscopy and/or flow
285 cytometry as described below.
286
287 **Confocal microscopy.** For no-wash imaging, a drop of sample (~5 µL) was taken directly from
288 the labeled culture. For wash imaging, cells were pelleted at 3300*g* for 3 min, washed twice with
289 1x Phosphate Buffered Saline (PBS) supplemented with 5% Tween80 (v/v), and resuspended in
290 300 µL 1x PBS. Subsequently, a drop of sample (~5 µL) was spotted onto a 1% agarose pad on
291 a microscope slide, allowed to dry, covered with a cover slip and sealed with nail polish.
292 Microscopy was performed on a Nikon A1R confocal microscope equipped with a Plan Fluor 60x
293 oil immersion (NA: 1.30) objective. Samples were excited with a 405-nm violet laser, 488-nm blue
294 laser, or 561-nm green laser and imaged in the Aqua Amine (425-475 nm), FITC/GFP (500-550
295 nm), or RFP (570-620 nm) channels, respectively. NIS-Elements AR software (Nikon Inc.) and
296 Fiji (ImageJ) v. 72 were used to process images. All image acquisition and processing were
297 executed under identical conditions for control and test samples.
298
299 **Flow cytometry.** Cells were pelleted at 3300*g* for 3 min, washed twice with 1x Dulbecco's
300 phosphate-buffered saline (DPBS; MT-21-030-CV, Thermo Fisher Scientific) supplemented with
301 5% Tween80 (v/v), and resuspended in 300 µL 1x DPBS. Fluorescence measurements were
302 taken in 5-mL culture tubes (14-959A, Thermo Fisher Scientific) suitable for flow cytometry.
303 Experiments were performed on a BD LSR II.UV instrument in the shared Fluorescence Activated
304 Cell Sorting (FACS) Facility at Stanford University. The instrument, excitation wavelengths, and
305 filter sets used are noted in each figure or figure caption. Data were obtained for 10,000 cells per
306 sample, processed using FlowJo, and imported into Prism 7 (Graphpad) for statistical analysis.
307

308 **Single-cell time-lapse microscopy.** Single-cell time-lapse imaging was achieved using a
309 microfluidic flow cell (CellASIC, B04A) and a custom temperature-controlled microscope system.
310 Samples of mid-log cultures (200 µL) were placed undiluted into loading wells. Wells containing
311 7H9 medium and 7H9 medium with dye were primed for 10 min at the target temperature under
312 5 psi. During the experiment, flow was set at 2 psi. Cells were imaged at 1-min time intervals
313 using a Ti-Eclipse stand (Nikon Instruments) with a Plan Apo 100X DM Ph3 (NA: 1.45) (Nikon)
314 objective and images were acquired with an iXon EM+ (Andor) camera. All cells were imaged in
315 phase-contrast and TIRF illumination. Cells stained with dyes excited at peak GFP wavelength
316 (488 nm; hydroxychromone dyes) were imaged under TIRF illumination to reduce background
317 signal and photobleaching, for which an OBIS laser (Coherent) light path was guided by an optical
318 fiber to a TIRF illuminator (Nikon) and focused on the sample. Temperature was maintained at 37
319 °C using a stage-top incubator (Haison) coupled to a heater-controller (Air-Therm). Timing and
320 control of the system was accomplished through µManager v. 1.41 (29).
321
322 **Image analysis.** Image stacks were imported into ImageJ (FIJI) for initial data processing.
323 Individual isolated cells were selected and cropped as image hyperstacks to include both phase-
324 contrast and fluorescence channels. Phase-contrast images were used for automated
325 segmentation analysis using Morphometrics (30) in MATLAB (Mathworks), and outlines were
326 overlaid on the corresponding fluorescence images for quantifying signal information. Further
327 analyses were carried out using custom MATLAB scripts. Cellular intensity was normalized to the
328 peak cellular intensity during labeling for dye constructs with high signal-to-background. The initial
329 period of fluorescence intensity decay was quantified by nonlinear regression fitting to an
330 exponential function ($I(t) = I_0 + I_1 e^{-\gamma t}$). For dye constructs with no signal, cellular intensity was
331 normalized by the mean signal-to-background of the cell to reflect the relative signal.
332
333 **Metabolic labeling of Mtb.** Mtb cultures were grown via inoculation of a 1-mL frozen stock into
334 50 mL of Middlebrook 7H9 liquid medium supplemented with 10% (v/v) OADC enrichment (BBL
335 Middlebrook OADC, 212351), 0.5% (v/v) glycerol, and 0.05% (w/v) Tween 80 (P1754, Sigma-
336 Aldrich) in a roller bottle. Cells were grown to an OD_{600} of 0.5 to begin the experiments. Cells were
337 incubated with 100 µM DMN-Tre or 10 µM 3HC3-Tre for the indicated times. Labeled cells were
338 harvested by centrifugation (3000*g* for 10 min) and then fixed in an equal volume of 4%
339 paraformaldehyde (cells were incubated at room temperature for 1 h, with occasional rotation of
340 the tube to ensure sterilization of all internal surfaces before fluorescence and flow cytometry
341 analysis)

342

343 ***Statistical analysis.*** Data are means ± SEM from at least two independent experiments. Unless
344 otherwise specified, all data were analyzed using GraphPad Prism software's ANOVA (analysis
345 of variance) test, as specified in the figure legends.

346

347 **ACKNOWLEDGEMENTS**

348 We thank M. Rajendram, D. M. Fox, and S. Banik for technical assistance and helpful discussions,
349 and A. Iavarone [QB3/Chemistry Mass Spectrometry Facility, University of California (UC),
350 Berkeley] for assistance with mass spectrometry. We also thank Aidan Pezacki for research
351 assistance. Flow cytometry was performed in the shared FACS facility at Stanford University on
352 equipment obtained with NIH S10 Shared Instrument grant S10RR027431-01. M.K. was
353 supported by the Stanford University's Diversifying Academia, Recruiting Excellence Fellowship,
354 and NIH Predoctoral Fellowship F31AI129359. S.G.L.K. was supported in part by a National
355 Science Foundation Graduate Research Fellowship (Grant No. DGE-1106400). K.C.H. is a Chan
356 Zuckerberg Biohub Investigator. This research was supported by the Allen Discovery Center at
357 Stanford on Systems Modeling of Infection (to K.C.H.), and grants from the Bill and Melinda Gates
358 Foundation (OPP115061) and NIH (AI051622) (to C.R.B.).

359 **FIGURES**

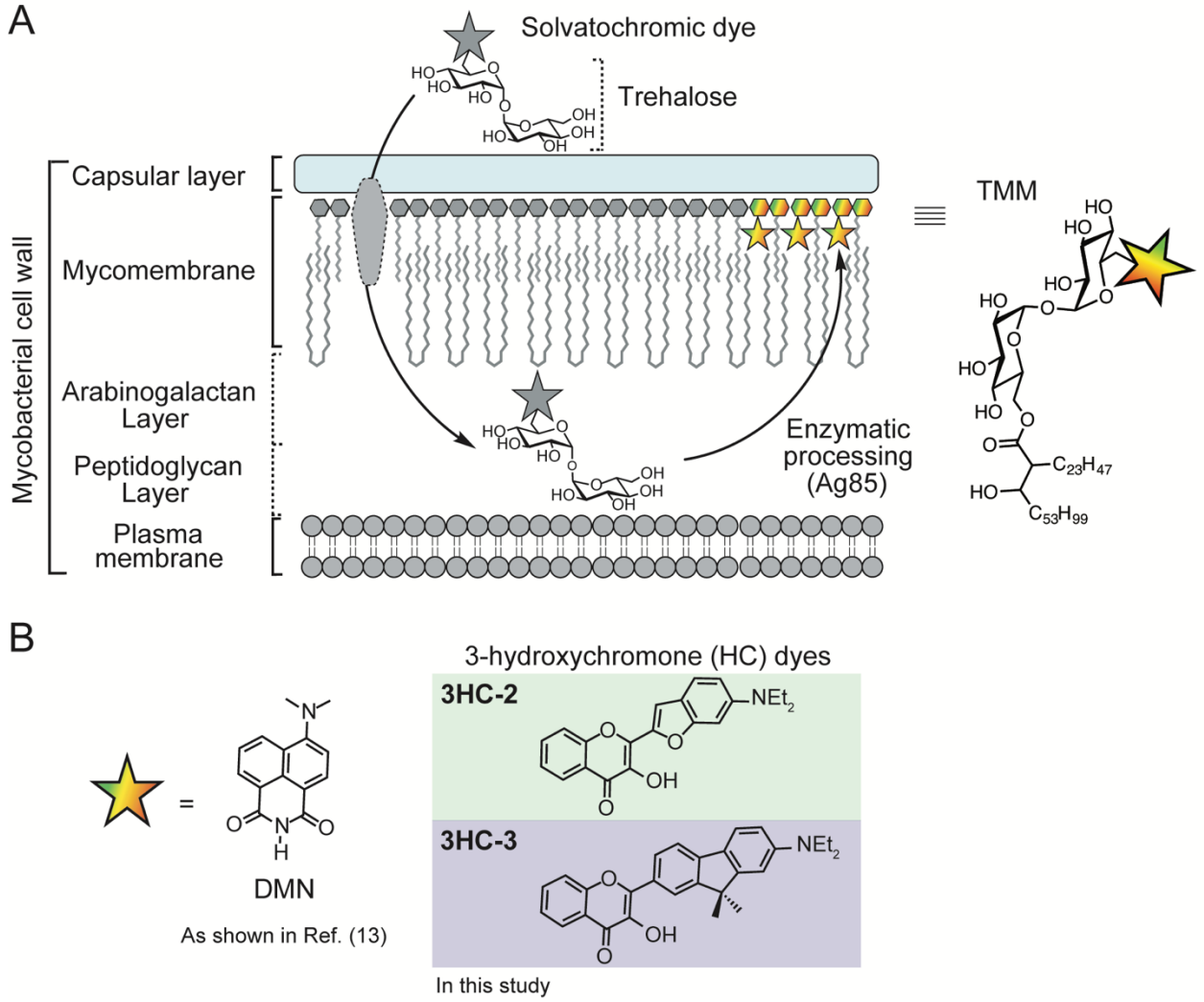

360

361 **Figure 1. Solvatochromic trehalose probes label the mycobacterial mycomembrane. (A)**
362 Solvatochromic trehalose probes are converted by mycobacteria to the corresponding trehalose
363 monomycolate (TMM, structure on right) analogs and inserted into the mycomembrane. There,
364 they undergo fluorescence turn-on, enabling detection of labeled cells by fluorescence
365 microscopy. **(B)** Chemical structures of solvatochromic dyes described in this study.

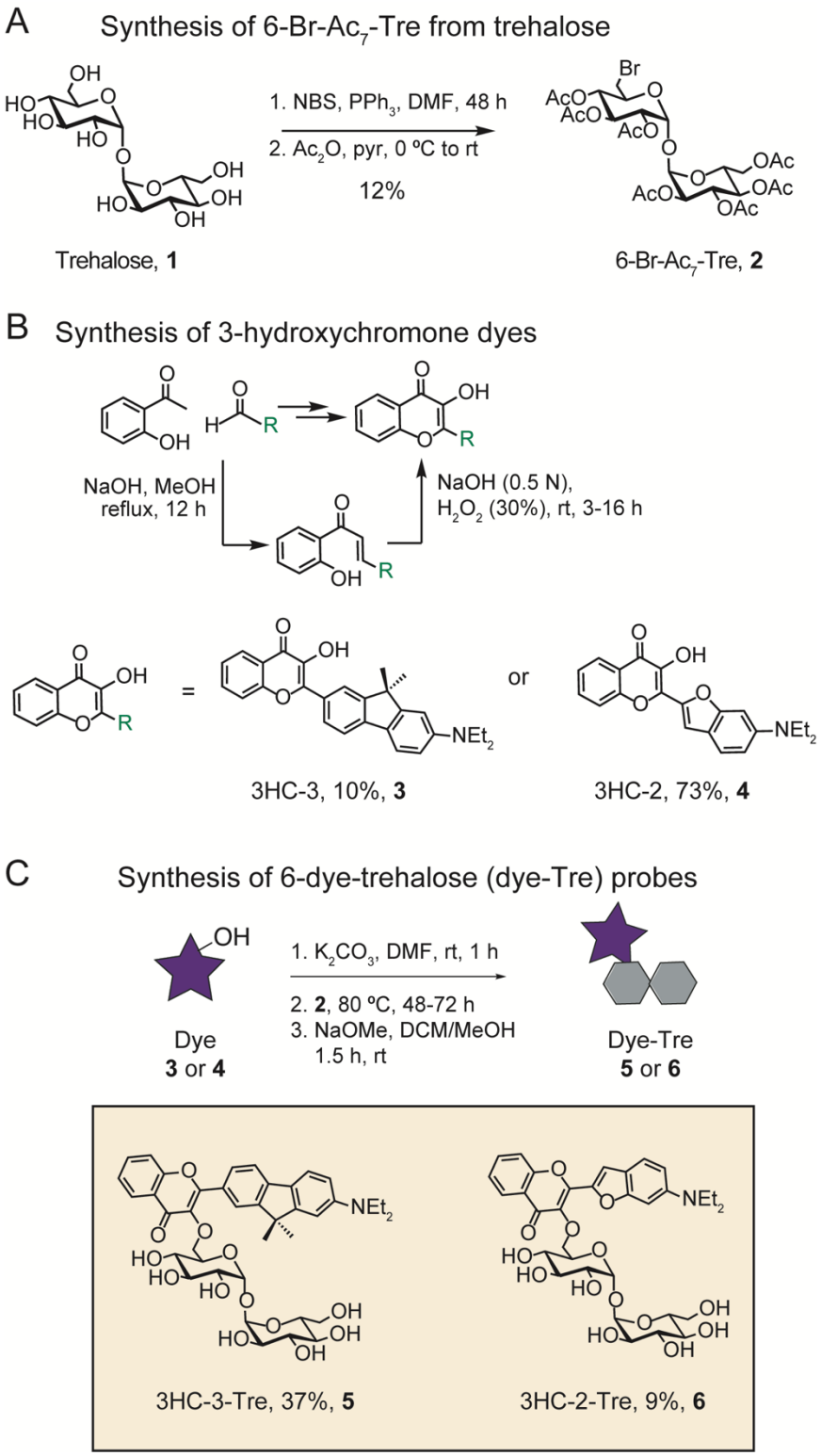

Figure 2. Synthetic scheme for 3-hydroxychromone (3HC) trehalose (Tre) dye conjugates.

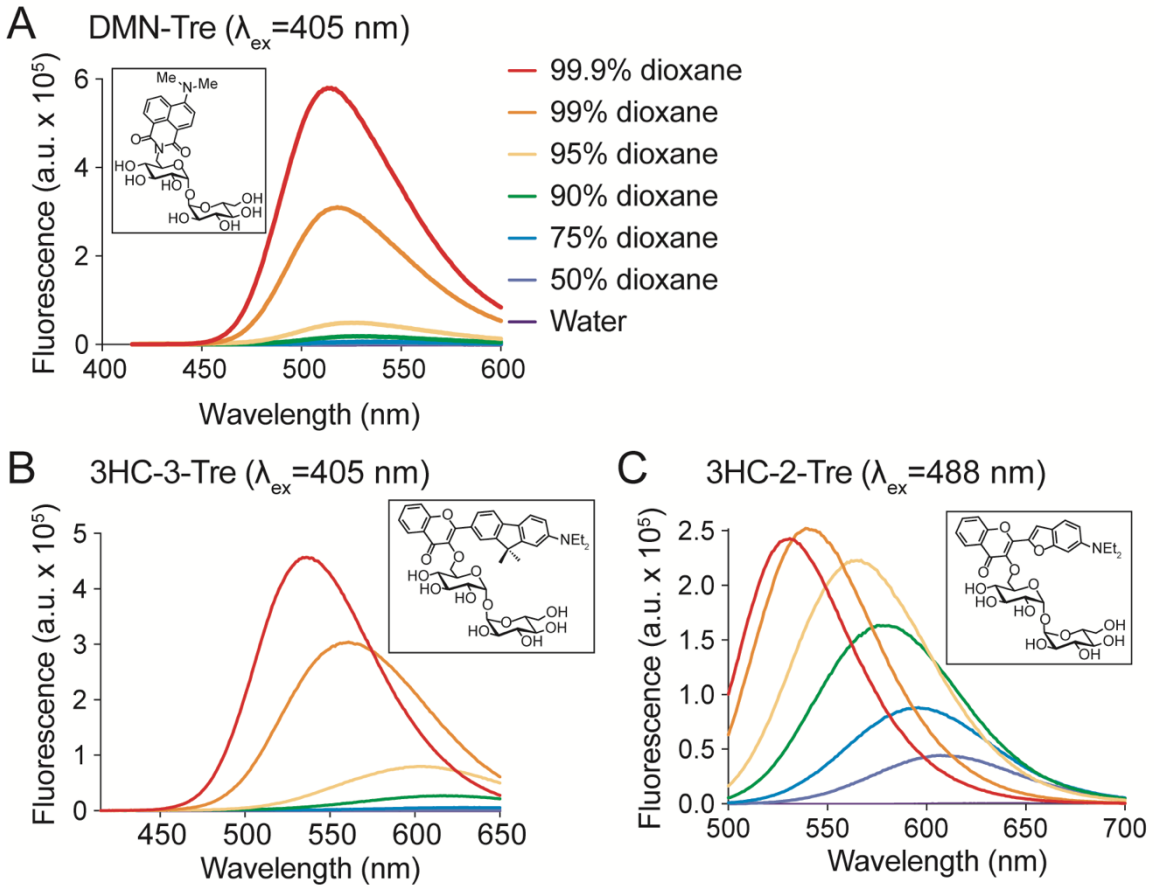

368

369 **Figure 3. Emission spectra of 3-hydroxychromone trehalose dyes.** Fluorescence spectra of
370 (**A**) DMN-Tre (ex. 405 nm), (**B**) 3HC-3-Tre (ex. 405 nm) and (**C**) 3-HC-2-Tre (ex. 488 nm) in
371 solvent systems with the indicated ratios of dioxane in water.

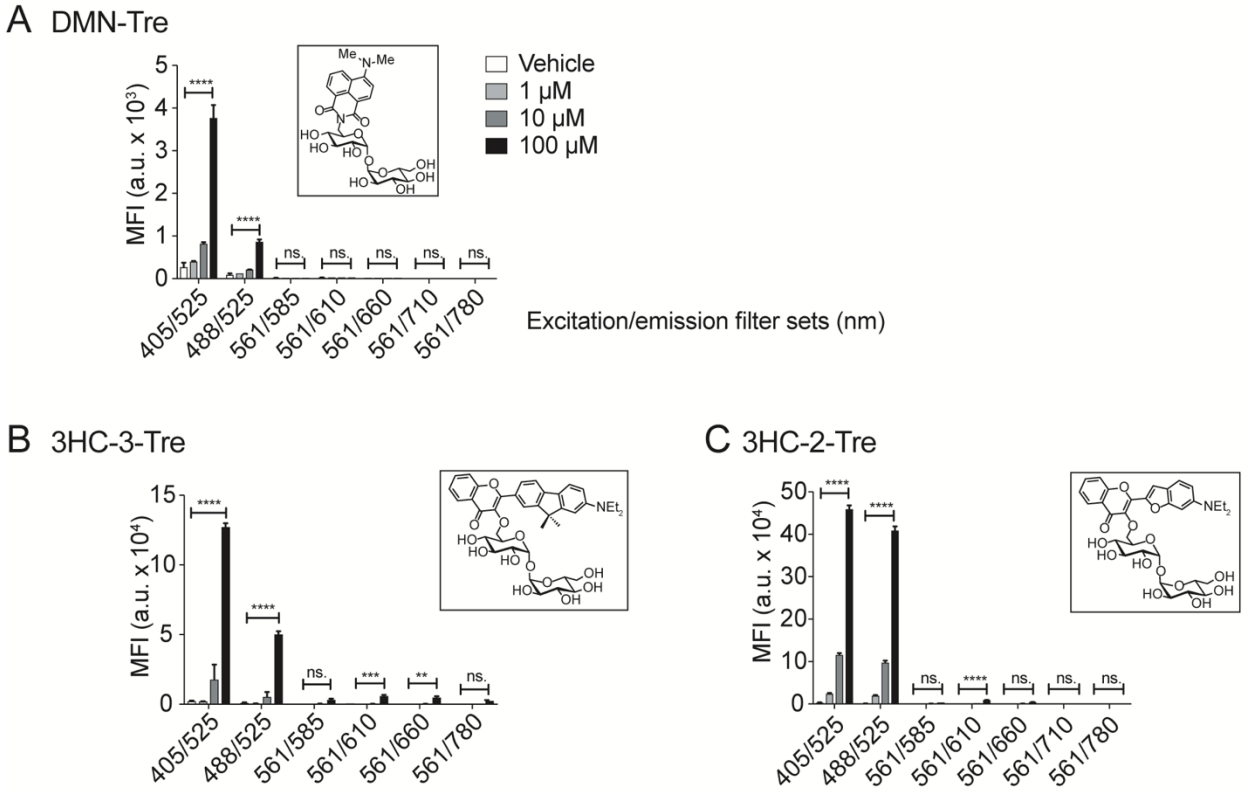

Figure 4. Flow cytometry analysis of Msmeg cells labeled with solvatochromic trehalose dyes using various excitation and emission filter sets. Flow cytometry analysis of Msmeg labeled with (**A**) DMN-Tre, (**B**) 3HC-3-Tre or (**C**) 3HC-2-Tre. All dyes showed increased labeling at the highest concentration (100 μM). Cells at OD_{600}=0.5 were incubated with the indicated dye-trehalose probe concentrations for 1 h at 37 °C. MFI = Mean fluorescence intensity. Data are means ± SEM from at least two independent experiments. Data were analyzed by two-way analysis of variance (ANOVA) test (*: p<0.05, **: p<0.01, ***: p<0.001, ****: p<0.0001, ns: not significant).

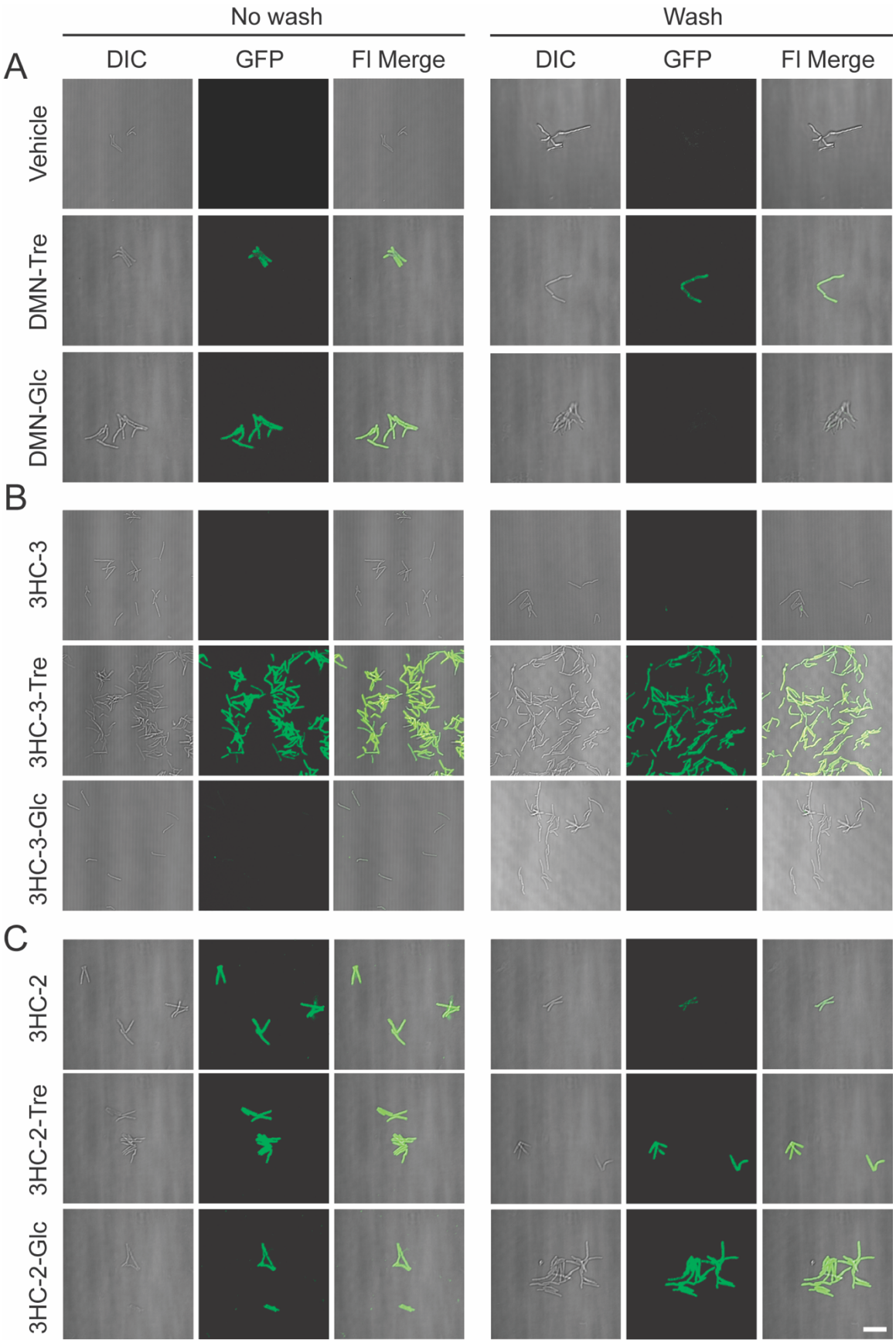
No wash
Wash
A
DIC
GFP
Fl Merge
DIC
GFP
Fl Merge
Vehicle
DMN-Tre
DMN-Glc
B
3HC-3
3HC-3-Tre
3HC-3-Glc
C
3HC-2
3HC-2-Tre
3HC-2-Glc

382 **Figure 5. Unlike 3HC-2-Tre, 3HC-3-Tre labeling is dependent on the trehalose moeity.**
383 Epifluorescence microscopy of Msmeg cells treated with (**A**) 100 μM DMN-Tre or DMN-Glc or no
384 dye control (Vehicle); (**B**) 100 μM of 3HC-3, 3HC-3-Tre, or 3HC-3-Glc; (**C**) 100 μM of 3HC-2, 3HC-
385 2-Tre, or 3HC-2-Glc. 3HC-3-Tre showed the most efficient labeling of Msmeg. Cells were
386 incubated with the indicated dyes for 1 h at 37 °C. Cells were smeared directly (No wash) or
387 washed 3 times with PBS then smeared onto a microscope slide (Wash). Scale bar: 10 μm.

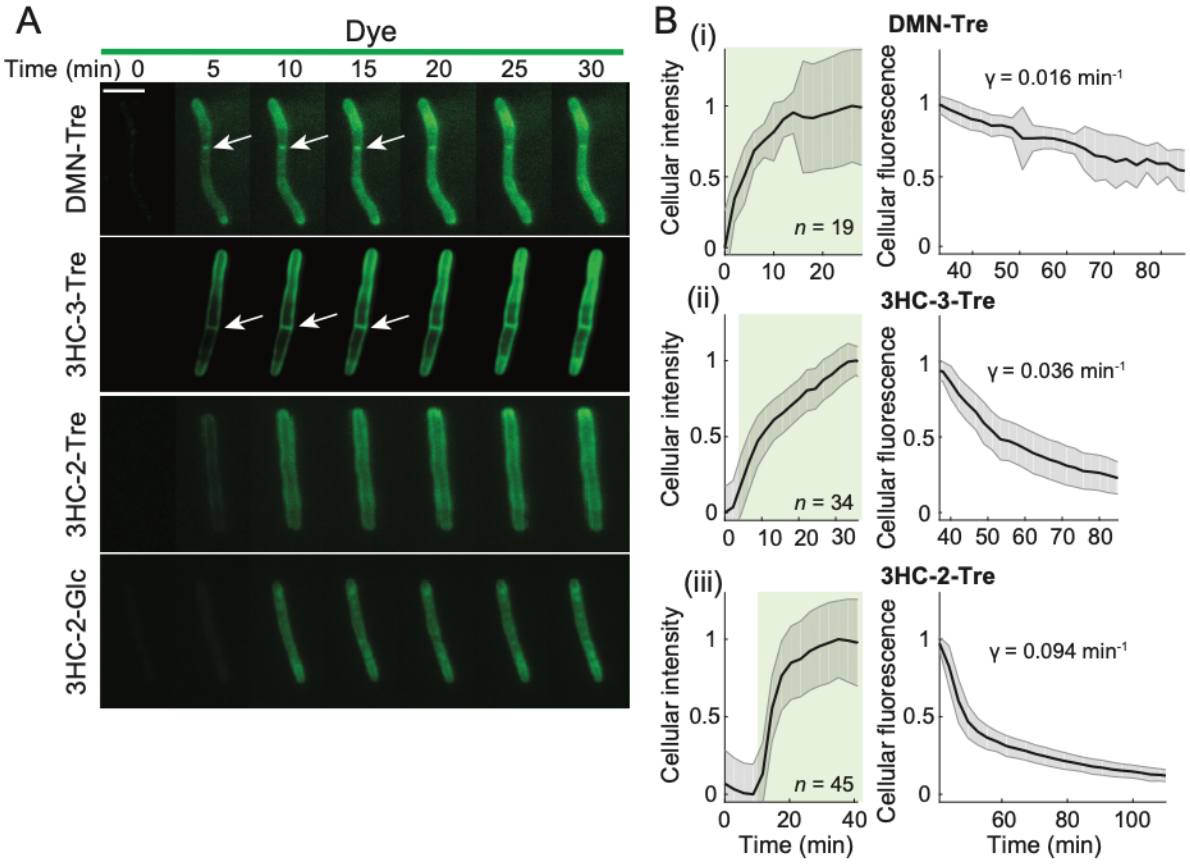

388

389 **Figure 6. Unlike 3HC-2 dye conjugates, 3HC-3-Tre labeling is initially localized at the**
390 **septum and poles.** (**A**) Time-lapse microscopy of Msmeg cells treated with 100 μM DMN-Tre,
391 3HC-3-Tre, 3HC-2-Tre, or 3HC-2-Glc for 30 min revealed concentration of 3HC-3-Tre at cell septa
392 and poles. White arrows denote septal labeling. Scale bar: 5 μm. (**B**) Quantitation of Msmeg
393 fluorescence in the presence of 100 μM (i) DMN-Tre, (ii) 3HC-3-Tre, or (iii) 3HC-2-Tre during
394 labeling for 30 min (left, volume-normalized intensity) and subsequent washing with growth
395 medium for 1 h (right, total fluorescence). The number of cells included in each analysis (*n*) is
396 provided in each panel. Shaded error bars represent ± 1 standard deviation.

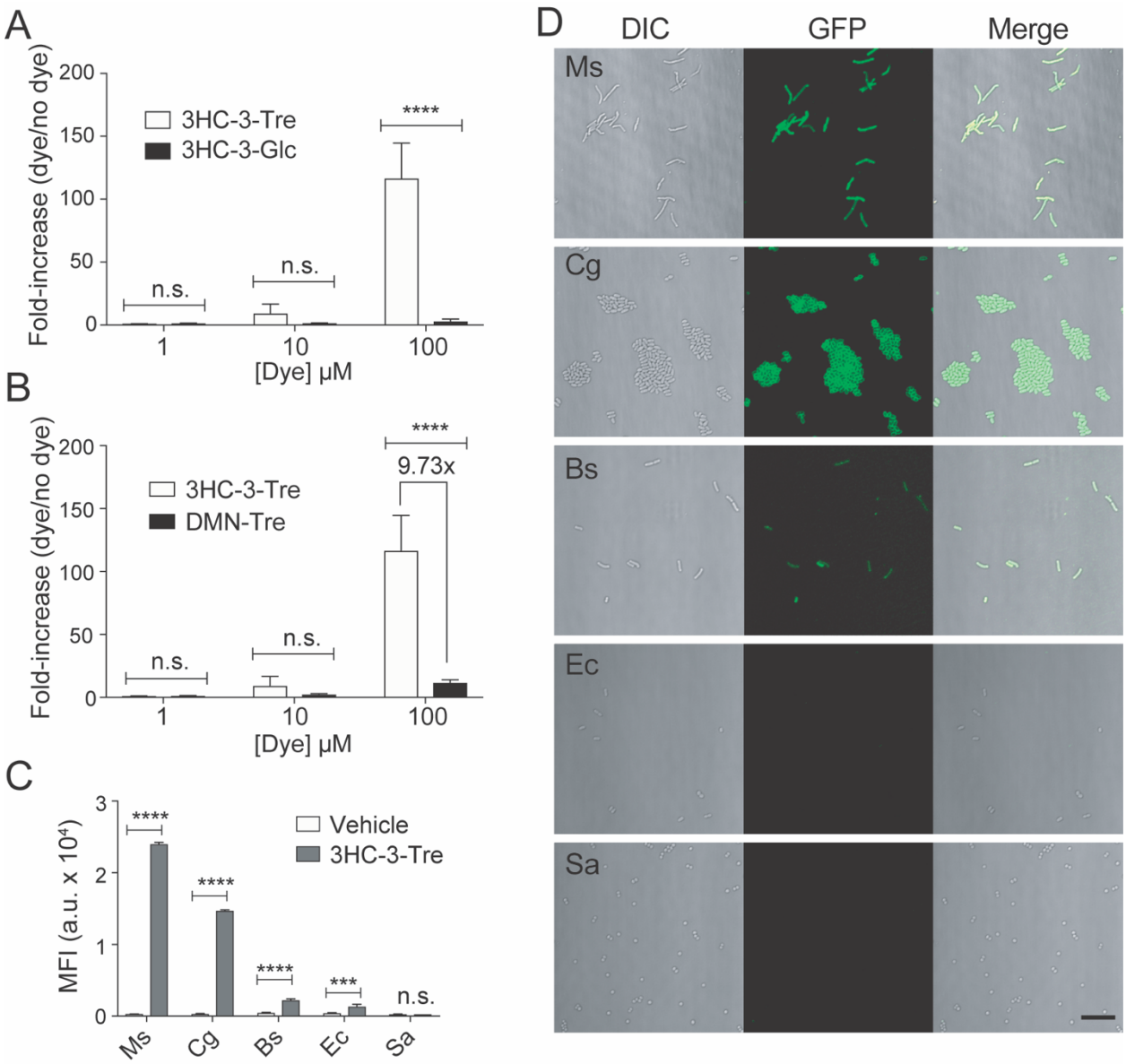

Figure 7. Specific labeling of live mycobacteria and corynebacteria with 3HC-3-Tre. (A,**B**) Flow cytometry analysis of Msmeg cells incubated for 1 h at 37 °C with (**A**) 100 μM 3HC-3-Tre or 3HC-3-Glc, (**B**) 100 μM 3HC-3-Tre or DMN-Tre. (**C**,**D**) Flow cytometry (**C**) and no-wash microscopy (**D**) analyses of Msmeg (Ms), *C. glutamicum* (Cg), *B. subtilis* (Bs), *E. coli* (Ec), and *S. aureus* (Sa) cells incubated for 1 h at 37 °C with 100 μM 3HC-3-Tre. 3HC-3-Tre labeling was specific to Msmeg and Cg. Data are means ± SEM from at least two independent experiments. Data were analyzed by two-way analysis of variance (ANOVA) test (*: $p<0.05$, **: $p<0.01$, ***: $p<0.001$, ****: $p<0.0001$, ns: not significant). Scale bar: 10 μm.

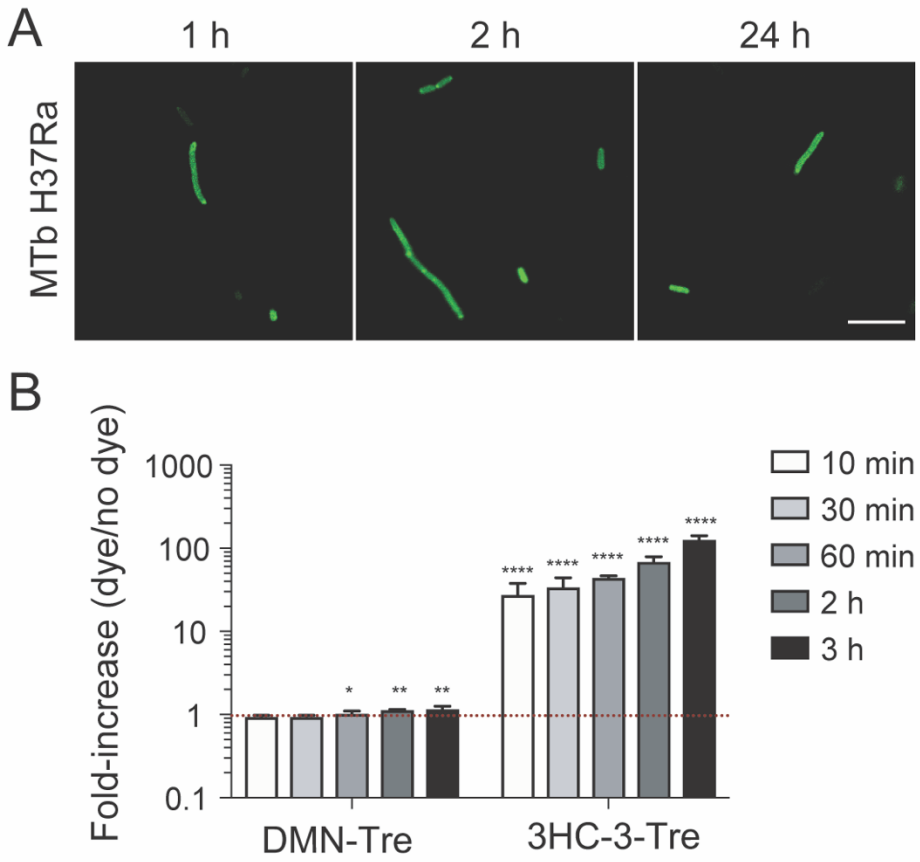

Figure 8. Mtb cells labeled with 3HC-3-Tre exhibit increased fluorescence intensities and can be detected within 10 minutes by flow cytometry. (**A**) Microscopy analysis of H37Ra Mtb cells labeled with 100 μM 3HC-3-Tre for 1, 2, or 24 h, followed by 4% paraformaldehyde fixation and fluorescence imaging. Scale bar: 10 μm. (**B**) Flow cytometry analysis of Mtb cells incubated for the indicated times with 100 μM DMN-Tre or 3HC-3-Tre, followed by 4% paraformaldehyde fixation. Ten minutes was sufficient for nearly complete labeling. Data are means ± SEM from at least two independent experiments. Data were analyzed by two-way analysis of variance (ANOVA) test (*: $p<0.05$, **: $p<0.01$, ***: $p<0.001$, ****: $p<0.0001$, ns: not significant).

REFERENCES

1. WORLD HEALTH ORGANIZATION. GLOBAL TUBERCULOSIS REPORT 2019. S.l.: WORLD HEALTH ORGANIZATION; 2019.

2. World Health Organization. High-priority target product profiles for new tuberculosis diagnostics: Report of a consensus meeting [Internet]. Geneva, Switzerland; 2014. Available from: https://apps.who.int/iris/bitstream/handle/10665/135617/WHO_HTM_TB_2014.18_eng.pdf?sequence=1

3. Singhal R, Myneedu VP. Microscopy as a diagnostic tool in pulmonary tuberculosis. *International Journal of Mycobacteriology*. **2015**, 4(1):1–6.

4. Ziehl F. Zur farbung des tuberkelbacillus. *Deutsche Medizinische Wochenschrift*. **1882**, 8:451.

5. Ziehl F. Ueber die Farbung des Tuberkelbacillus. *Deuts Med Wchr*. **1883**, 9:247–9.

6. Neelsen F. Ein Casuistischer Beitrag zur Lehre von der Tuberkulose. *Centralblatt für die Medizinischen Wissenschaften*. **1883**, 28:497–501.

7. Hagemann PK. Fluoreszenzfärbung von Tuberkelbakterien mit Auramin. *Münchener Medizinische Wochenschrift.* **1938**, 85:1066–8.

8. Boyd JC, Marr JJ. Decreasing reliability of acid-fast smear techniques for detection of tuberculosis. *Ann Intern Med*. **1975**, 82(4):489–92.

9. Truant JP, Brett WA, Thomas W. Fluorescence microscopy of tubercle bacilli stained with auramine and rhodamine. *Henry Ford Hosp Med Bull.* **1962,** 10:287–96.

10. Belisle JT, Vissa VD, Sievert T, Takayama K, Brennan PJ, Besra GS. Role of the Major Antigen of Mycobacterium tuberculosis in Cell Wall Biogenesis. *Science*. **1997**, 276(5317):1420–2.

11. Swarts BM, Holsclaw CM, Jewett JC, Alber M, Fox DM, Siegrist MS, et al. Probing the Mycobacterial Trehalome with Bioorthogonal Chemistry. *J Am Chem Soc*. **2012,** 134(39):16123–6.

441 12. Foley HN, Stewart JA, Kavunja HW, Rundell SR, Swarts BM. Bioorthogonal Chemical
442 Reporters for Selective In Situ Probing of Mycomembrane Components in Mycobacteria.
443 *Angewandte Chemie International Edition*. **2016**, 55(6):2053–7.

444 13. Backus KM, Boshoff HI, Barry CS, Boutureira O, Patel MK, D'Hooge F, et al. Uptake of
445 unnatural trehalose analogs as a reporter for *Mycobacterium tuberculosis*. *Nature Chemical*
446 *Biology*. **2011,** 7(4):228–35.

447 14. Rundell SR, Wagar ZL, Meints LM, Olson CD, O'Neill MK, Piligian BF, et al. Deoxyfluoro-D-
448 trehalose (FDTre) analogues as potential PET probes for imaging mycobacterial infection.
449 *Org Biomol Chem*. **2016**, 14(36):8598–609.

450 15. Barry C. Exploiting the biology of trehalose to develop novel imaging probes for tuberculosis.
451 *The FASEB Journal*. **2016**, 30(1_supplement):503.1-503.1.

452 16. Rodriguez-Rivera FP, Zhou X, Theriot JA, Bertozzi CR. Visualization of mycobacterial
453 membrane dynamics in live cells. *J Am Chem Soc*. **2017**, 139(9):3488–95.

454 17. Hodges HL, Brown RA, Crooks JA, Weibel DB, Kiessling LL. Imaging mycobacterial growth
455 and division with a fluorogenic probe. *Proc Natl Acad Sci USA*. **2018**, 115(20):5271–6.

456 18. Cheng Y, Xie J, Lee K-H, Gaur RL, Song A, Dai T, et al. Rapid and specific labeling of single
457 live *Mycobacterium tuberculosis* with a dual-targeting fluorogenic probe. *Sci Transl Med.*
458 **2018,** 10(454).

459 19. Kamariza M, Shieh P, Ealand CS, Peters JS, Chu B, Rodriguez-Rivera FP, et al. Rapid
460 detection of Mycobacterium tuberculosis in sputum with a solvatochromic trehalose probe.
461 *Science Translational Medicine.* **2018,** 10(430):eaam6310.

462 20. Klymchenko AS, Mely Y. Fluorescent environment-sensitive dyes as reporters of
463 biomolecular interactions. *Prog Mol Biol Transl Sci*. **2013**, 113:35–58.

464 21. Sahile HA, Rens C, Shapira T, Andersen RJ, Av-Gay Y. DMN-Tre Labeling for Detection and
465 High-Content Screening of Compounds against Intracellular Mycobacteria. *ACS Omega*.
466 **2020**, 5(7):3661–9.

467 22. McLean AM, Socher E, Varnavski O, Clark TB, Imperiali B, Goodson T. Two-photon
468 fluorescence spectroscopy and imaging of 4-dimethylaminonaphthalimide peptide and
469 protein conjugates. *J Phys Chem B*. **2013**, 117(50):15935–42.

470 23. Klymchenko AS, Pivovarenko VG, Ozturk T, Demchenko AP. Modulation of the solvent-
471 dependent dual emission in 3-hydroxychromones by substituents. *New J Chem.* **2003**,
472 27(9):1336–43.

473 24. Kucherak OA, Richert L, Mély Y, Klymchenko AS. Dipolar 3-methoxychromones as bright and
474 highly solvatochromic fluorescent dyes. *Phys Chem Chem Phys.* **2012,** 14(7):2292–300.

475 25. Kucherak OA, Didier P, Mély Y, Klymchenko AS. Fluorene Analogues of Prodan with Superior
476 Fluorescence Brightness and Solvatochromism. *J Phys Chem Lett.* **2010**, 1(3):616–20.

477 26. Klymchenko AS, Ozturk T, Pivovarenko VG, Demchenko AP. A 3-hydroxychromone with
478 dramatically improved fluorescence properties. *Tetrahedron Letters*. **2001**, 42(45):7967–70.

479 27. Gunduz S, Goren AC, Ozturk T. Facile Syntheses of 3-Hydroxyflavones. *Org Lett.* **2012**,
480 14(6):1576–9.

481 28. Junior COR, Castro SBR, Pereira AA, Alves CCS, Oliveira EE, Rêgo RT, *et al.* Synthesis of
482 genistein coupled with sugar derivatives and their inhibitory effect on nitric oxide production
483 in macrophages. *European Journal of Medicinal Chemistry*. **2014**, 85:615–20.

484 29. Edelstein A, Amodaj N, Hoover K, Vale R, Stuurman N. Computer Control of Microscopes
485 Using μManager. *Current Protocols in Molecular Biology*. **2010,** 92(1):14.20.1-14.20.17.

486 30. Ursell T, Lee TK, Shiomi D, Shi H, Tropini C, Monds RD, et al. Rapid, precise quantification
487 of bacterial cellular dimensions across a genomic-scale knockout library. *BMC Biology*. **2017**,
488 15(1):17.

489